Article

Pressure Drops in Two-Phase Gas–Liquid Flow through Channels Filled with Open-Cell Metal Foams

Roman Dyga [1],* and **Sebastian Brol** [2]

[1] Department of Process and Environmental Engineering, Faculty of Mechanical Engineering, Opole University of Technology, Mikołajczyka 5, 45-271 Opole, Poland

[2] Department of Vehicles, Faculty of Mechanical Engineering, Opole University of Technology, Mikołajczyka 5, 45-271 Opole, Poland; s.brol@po.edu.pl

* Correspondence: r.dyga@po.edu.pl

Abstract: This paper describes experimental investigations of single-phase and two-phase gas–liquid flow through channels with a diameter of 20 mm and length of 2690 mm, filled with metal foams. Three types of aluminium foams with pore densities of 20, 30 and 40 PPI and porosities ranging from 29.9% to 94.3% were used. Air, water and oil were pumped through the foams. The tests covered laminar, transitional and turbulent flow. We demonstrated that the Reynolds number, in which the hydraulic dimension should be defined based on foam porosity and pore diameter $d_e = \phi d_p/(1 - \phi)$, can be used as a flow regime assessment criterion. It has been found that fluid pressure drops when flowing through metal foams significantly depends on the cell size and porosity of the foam, as well as the shape of the foam skeleton. The flow patterns had a significant influence on the pressure drop. Among other things, we observed a smaller pressure drop when plug flow changed to stratified flow. We developed a model to describe pressure drop in flow through metal foams. As per the proposed methodology, pressure drop in single-phase flow should be determined based on the friction factor, taking into account the geometrical parameters of the foams. We propose to calculate pressure drop in gas–liquid flow as the sum of pressure drops in gas and liquid pressure drop corrected by the drop amplification factor.

Keywords: gas–liquid flow; single flow; pressure drop; open-cell metal foam; modelling the pressure drop; flow patterns

1. Introduction

Many industrial processes use an apparatus with structured packing. Open-cell metal foams can play the role of the packing. Metal foam is a special cellular material in which the metal takes the form of a spatial skeleton, formed by thin ligaments. The ligaments form the outer outline of adjacent hollow cells. The cell size can be up to an order of magnitude larger than the transverse skeleton ligament size, giving foams a very high porosity, typically over 90%. High porosity coupled with a lack of closed cells allows relatively free flow of fluids through the foams. Due to small pressure drop after flowing through foams, their large specific surface area and the high thermal conductivity of the skeleton, the foams are increasingly being considered as an alternative to other structured packings. In many cases, the use of foams allows achieving beneficial energy effects in the form of reduced energy consumption for pumping fluids or increased heat and mass transport intensity. As a consequence, the efficiency of apparatuses is increased. The benefits of using foams in the construction of process equipment have also been noted in processes involving two-phase gas–liquid mixtures. What has been mostly studied so far, were boiling processes in channels completely or partially filled with metal foams. Works in this area have been carried out for several years. The authors of [1,2] have shown that the presence of foam on the boiling surface reduces the vapour bubbles nucleation temperature and shifts the boiling crisis towards much higher heat flux densities. Hu et al. [3] report

that the heat transfer coefficient recorded when during flow of boiling refrigerant through the channels of refrigeration evaporators filled with foam is 1.5 to 4 times higher than for boiling in evaporators without foam. In similar refrigerant boiling studies conducted by Bamorovat Abadi et al. [4] and Li et al. [5], the heat penetration rate increased by 3.2 and 2.5–3 times, respectively.

Diani et al. [6] and Zhu et al. [7] emphasise that the application of foam to the boiling surface is most beneficial when the process is carried out at a flow with low mass flux of the fluid and high vapour quality. According to Wang et al. [8], the increase in heat transfer intensity is due to induced flow disturbances in the boundary layer, more intensive mixing of vapour and liquid and increased effective thermal conductivity. Kouidri and Madani [2] also noted the great importance of thermal conductivity. These authors have shown that when boiling in a channel filled with highly conductive copper foam, heat transport increases by 130 to 300%, with an average increase in pressure drop by 42%. Foams made of materials with lower thermal conductivity (NiFeAlCr alloy and Inconel) placed in the channel caused a deterioration in heat transport compared to boiling in an empty channel.

The apparatus energy efficiency largely depends on the energy required to pump the fluids. According to Lali [9], for this energy, there is a small flow through metallic foams. In his study, it did not exceed 1 W/m^3, for foams with pore packing densities of 30 and 45 PPI o. Jamal-Abdad et al. [10] estimate that the thermal efficiency of solar collectors after filling their evaporators with copper foam increases by up to 45% compared to collectors without foam. When studying condensation in a tube with an annular copper foam insert, Shi et al. [11] recorded 30% higher energy efficiency than in a tube with microribs. On the contrary, in a study of subcooled flow boiling in a duct filled with copper foam [12], the authors recorded a 22% increase in the energy efficiency of the process.

As assessed by Hu et al. [13], the pressure drop in boiling R410A refrigerant increases with increasing mass flux and when vapor quality increases. Similar observations were made by Ji and Xu [14]. They recorded linear changes in pressure drop as a function of vapour mass fraction and higher pressure drop values for foams with higher pore packing density. Zalucky et al. [15] have shown that pressure drop for gas–liquid flow through a packed bed of metal foam is several times lower than for flow through a spherical packed bed of the same specific surface.

Studies of gas–liquid co-current flow through metal foams in processes other than boiling or condensation are mainly related to the use of foams in catalytic reactors fuel cells and packed columns. An overview of the topics and test conditions for gas–liquid flows other than liquid–vapour flow is given in Table 1.

Chen et al. [16] used nickel foam as a catalyst carrier in a micro-reactor. They found that the process of nitrobenzene hydrogenation in this reactor s more efficient than in a conventional reactor in which the catalyst is applied to the inner walls. The authors of [16] found that mass transport increased multiple times due to the very large foam surface area and flow disturbances around the foam skeleton. Bao et al. Based on the results of a numerical analysis of gas and liquid flow through a PEMFC membrane fuel cell, [17] found that the presence of foam in the flow field results in a more uniform distribution of gas to the electrodes than in cells with conventional parallel channels. However, the foam causes a greater hold-up of liquid droplets that become trapped in its cells, so it is necessary to use hydrophobic foams to prevent clogging. Li et al. [18] pointed to similar issues when studying air–water flow through a T-junction channel filled with metal foam. The authors of [18] found that water is retained in one of the tee arms and that this retention effect is enhanced when the pore packing density of the foam is increased. Water retention can cause a change in flow pattern, from annular to slug.

As well as in the case of the flow in the empty channels [19] the flow through the metal foam was studied using neural network [20,21]. The papers devoted inter alia hydrodynamics phenomena, but pressure drop was not their subject.

Table 1. Overview of studies on gas and liquid flow through channels filled with metal foams. Papers not dealing with boiling or condensation.

Reference	Research Contents	Fluids	Foam Pore Density/Porosity	Scope of the Study
Bao et al. [17]	Numerical simulation of gas–liquid flow in a fuel cell	air, water	10 PPI/0.94 40 PPI/0.97	velocity and pressure field, water droplets hold-up
Chen et al. [22]	horizontal co-current flow through microreactor	hydrogen, aqueous ethanol	35 PPI/0.90 75 PPI/0.89 110 PPI/0.90	nitrobenzene conversion and phase distribution
Li et al. [18]	flow in a mini-T-junction	air, deionized water	10 PPI/– 20 PPI/–	phase split,
Tourvieille et al. [23]	horizontal co-current flow through microreactor	hydrogen, ethanol, methanol	35 PPI/0.90 45 PPI/0.89 55 PPI/0.90	mass transfer and pressure drop
Wan et al. et al. [24]	horizontal co-current flow through a fuel cell	air, water	110 PPI/0.95	flow field and temperature distribution
Zalucky et al. [15]	gas–liquid downflow in solid foam packed trickle bed reactors	Air, water	20 PPI/0.87 30 PPI/0.89 45 PPI/0.85	flow patterns, liquid holdup and axial pressure drop

1.1. Mathematical Description of Pressure Drop in Gas–Liquid Flow

Despite a growing number of papers devoted to the use of metal foams in the construction of process equipment being found in the literature, mathematical descriptions of phenomena accompanying gas–liquid flows through foams are very limited. This also applies to the description of pressure drop. Table 2 summarises the approach of various researchers to modelling pressure drop in gas–liquid flow in channels and equipment filled with open-cell metal foams.

According to Gao et al. [25], the frictional pressure drop in boiling refrigerant in a duct filled with foam can be calculated in the same way as for an empty duct, using the Faning friction factor, but the number they defined empirically is only valid for the foam used in their study.

Gerbaux et al. [26] propose determining pressure drop in gas–liquid flow using the Darcy-Forchheimer-Brinkman equation, which is applicable to single-phase flow through porous media. For two-phase flow, the authors of [26] introduced correction factors for the permeability and inertial coefficient of the foam into this equation.

Kouiduri and Madani [2] argue that methods used to calculate pressure drop in gas–liquid flow in hollow channels should not be applied to flow through metallic foams. The attempt at using the Lockhart-Martinelli method, the Bankoff method and the Friedel method in their original forms described by these researchers shows too large discrepancies in the calculated and measured pressure drop values. According to the authors of [13,14], the Lockhart-Martinelli method can be used to calculate pressure drop in boiling refrigerants flowing through solid foams, but only after making suitable adaptations.

Hu et al. [13] indicate that pressure drop in the fluid flow should be determined using the Ergun's equation, which is appropriate for flow through granular beds. The foam specific surface area, porosity and pore diameter should be given as parameters characterising the bed. Shi et al. [11] propose the same solution for calculating pressure drop at condensation, however, the authors empirically determined their constants for the calculation model, as their research concerned a duct only partially filled with foam.

A similar solution was developed by Ji and Xu [14]. In their proposal, pressure drop for fluid flow is determined based on the pressure drop number for flow through metal foams.

Table 2. Mathematical description of the pressure drop in two-phase gas–liquid flow through metal foams presented in the literature. (Correlations describing pressure drop in gas–liquid and single-phase flow are presented in Table 6).

Reference	Two-Phase Model	Single-Phase Pressure Drop	Applicability and Limitations
Bamorovat Abadi et al. [27]	Homogeneous flow in empty channel with the Chisholm's two-phase friction multiplier	Friction factor for homogeneous flow according to the Blasius and Hagen–Poiseuillw correlation	Flow boiling of refrigerant in a mini-channel Mass flux: 400–700 kg/(m²·s), Vapor quality: 0.1–0.7 Heat flux: 20–40 kW/m²,
Gao et al. [25]	Homogeneous flow	A correlation between the Faning factor and the Reynolds number fitted to experimental data	Flow boiling of refrigerant in a mini-channel Valid for the foam used in the study [25]
Hu et al. [13]	Separated flow, Lockhart-Martinelli model with Chisholm's formula $C = f(g_{2f}, d_p, x, \omega)$	Ergun equation Geometry model of foam by Inayat [28]	Flow boiling of the refrigerant-oil mixture Mass flux: 30–90 kg/(m²·s), Vapor quality: 0.2–0.8 Oil concentration: 0–5%
Ji and Xu [14]	Separated flow, Lockhart-Martinelli model with Chisholm's formula $C = f(g_{2f}, d_p, x)$	An experimental correlation considering the effects of change vapor qualities, mass fluxes and pore diameters. Faning factor correlation fitted to experimental data	Boiling flow in a rectangular channel. Laminar flow.
Shi et al. [11]	Separated flow, Lockhart-Martinelli model with Chisholm's formula $C = f(g_g, d_c, x)$	Ergun equation Geometry model of foam by Inayat [28]	Flow condensation in horizontal tubes filled with annular metal foam
Tourvieille et al. [23]	Separated flow, Lockhart-Martinelli model with Chisholm's formula.	The sum of the pressure drop of liquid in empty channel and channel with the foam. The pressure drop of liquid in a channel filled according to Darcy's law	Gas-liquid flow in microreactor Taylor flow $v_{sl} < 0.25$ m/s
Weise et al. [29]	Combining the homogeneous model for two-phase pressure drop in empty channel and the single-phase model flow in porous media	Forchheimer equation without Darcy term. Forchheimer coefficients known from single-phase experiments	Flow boiling Mass flux: >25 kg/(m²·s), Vapor quality < 0.5 Forchheimer number Fo < 10 Incompressible vapor phase—Ma^V < 0.1

One of the most recent methods for calculating pressure drop in gas–liquid flow through metal foams was presented by Weise et al. [29]. The authors propose to use the homogeneous flow model in hollow tubes in combination with the Forchheimer equation, which describes the pressure drop in single-phase flow through porous media. Weise et al. have shown that the Darcy term can be neglected in the Forchheimer equation for typical boiling. The influence of the channel wall is also negligible if the characteristic length scale of the channel exceeds the characteristic microscopic length scale of the foam by more than five times. The authors of [29] assure that the computational model proposed by the allows the determination of pressure drop with an error of less than 30% if the value of the Forchheimer coefficient for the foam has been experimentally determined. When the

Forchheimer coefficient needs to be predicted, the accuracy of the model decreases and depends on the accuracy of the models describing the value of the Forchheimer coefficient. Then, the knowledge of the geometrical foam parameters such as specific surface area, porosity, fibre diameter and pore diameter, becomes necessary.

1.2. Research Rationale and Objectives

The literature review suggests that studies of pressure drop in gas–liquid flow through channels filled with metal foams mostly concern the flow of boiling agents in evaporators of refrigerating appliances and solar collectors. These works resulted, among other things, in the development of correlations used for the prediction of pressure drop in such flows. However, these correlations do not apply to two-phase flows other than boiling. The results of statistical verification of these correlations based on the measurement results described in this paper, presented in Section 4, confirm this.

Co-current gas–liquid flow through channels filled with metal foams with gases different from liquid vapour has so far been studied only in channels of small diameters, in microreactors and fuel cells (leaving aside flows in packed columns which are diametrically different processes). Mass transport and the quantities characterising the mass exchange processes were the most frequent subject of investigations. Studies on flow hydrodynamics are less frequent and they usually concern the liquid hold-up on the foam or the determination of the velocity field. In a few cases, the authors discussed pressure changes, but a method for predicting pressure drop in two-phase flow was proposed only by Tourvieille et al. [23]. The authors of the [23] paper conducted their study only in the laminar regime at very low flow velocities.

The literature is missing data on the influence of flow patterns in foam-filled channels on pressure drop (apart from flow boiling).

In cases other than refrigerant boiling, the scarcity of information on gas–liquid flows through open-cell metal foams, including the lack of methods for predicting pressure drop, severely hinders the design and optimisation of apparatuses filled with metal foams. Therefore, we engaged in our research, including experimental studies, aimed at understanding the hydrodynamics of gas–liquid flow through channels filled with metal foams, with particular emphasis on the factors determining pressure drop in two-phase flow, including flow conditions, fluid properties and foam structure.

In contrast to the authors of earlier work, we engaged in investigating flow in conventional channels (circular with a diameter of 20 mm) in not only laminar but also turbulent regime. We found that pressure drop was related to flow patterns.

The necessity to develop a new model for predicting the value of pressure drop in gas–liquid flow through the open-cell metal foam, which would correctly describe this value for various flow patterns and could be applied in flow conditions where literature models are not applicable, was deemed a useful objective of the works we engaged in.

2. Materials and Methods

The direct aim of the experimental research was to measure pressure drop in single-phase and two-phase gas–liquid flow through channels filled with metal foams of open structure. For two-phase flow, we also identified flow patterns to determine their influence on pressure drop values. Single-phase flow through open cell foams is relatively well understood [30–32], however, it was considered that the results of single-phase flow research would help interpret the more complex two-phase flow. It is not always possible to rely solely on literature information. The authors of individual papers often describe the foams used in their research in an insufficiently precise manner, for example, using only one quantity to characterise their geometrical structure. A uniform methodology for determining geometric foam parameters has still not been developed. The ways of defining the Reynolds number and, consequently, the criteria for assessing flow regime also differ, which makes it difficult to analyse and compare the research results presented in the literature and to make the necessary generalisations.
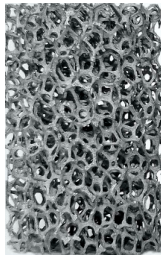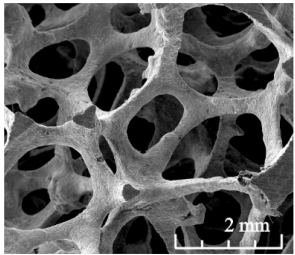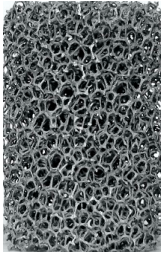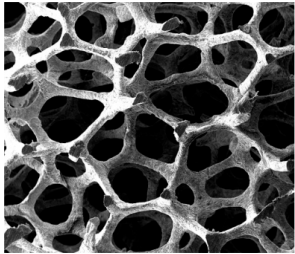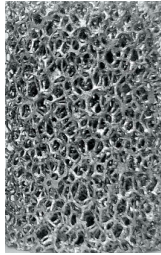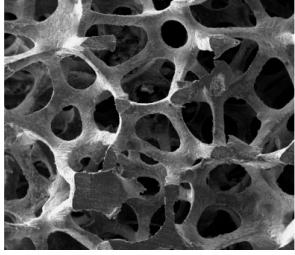
Air, demineralised water and Velol-9Q oil were used as fluids. Studies of gas–liquid flow through metal foams reported in the literature have mostly been conducted using refrigerants or air and water. The use of oil introduced more diversity in the physical properties of the fluids and thus allowed to determine their influence on hydrodynamic phenomena. Velol-9Q oil is significantly more viscous than that of water, eight times at 20 °C, but this viscosity is still low enough to carry out tests over a wide range of fluid velocity changes. Oil properties are shown in Table 3 (the properties of air and water are generally known and available). The two-phase flow was analysed for the air–water and air–oil flows.

Table 3. Characteristics of oil Velol-9Q.

Property	Dependence on Temperature
viscosity μ, Pa·s	$\mu = 0.1172t^{-0.865}$
density ρ, kg/m^3	$\rho = 875.03 - 0.783t + 0.0012t^2$

Three aluminium open-cell foams with different pore densities of 20, 30 and 40 PPI were used in the study. Foams with lower pore density, e.g., 5 or 10 PPI, are characterised by a relatively small specific surface area, usually smaller than other packings used in heat or mass transfer processes. Foams with too high pore density induce extensive pressure drop, which outweighs the benefits associated with their use in process equipment. The foams exhibited similar porosity ϕ and cell skeleton shape. They differed in cell size. Some foam parameters needed to be similar to unambiguously assess the influence of fluid properties on flow hydrodynamics. The foam parameters and geometrical structure are presented in Table 4.

Table 4. Characteristics of aluminium foams.

| Morphological Parameters	Foam View	Microscopic Image (Magnification ×15)
foam 20 PPI (m-pore) porosity $\phi = 0.934$ cell diameter $d_c = 3.45 \cdot 10^{-3}$ m pore diameter $d_p = 1.09 \cdot 10^{-3}$ m		
foam 30 PPI (m-pore) porosity $\phi = 0.943$ cell diameter $d_c = 2.25 \cdot 10^{-3}$ m pore diameter $d_p = 0.71 \cdot 10^{-3}$ m		
foam 40 PPI (Duocell) porosity $\phi = 0.929$ cell diameter $d_c = 2.38 \cdot 10^{-3}$ m pore diameter $d_p = 0.82 \cdot 10^{-3}$ m		

Foam porosity ϕ was determined based on the equation

$$\phi = 1 - \frac{V_s}{V_{mf}},\tag{1}$$

where V_{mf} is the volume of the foam sample in the form of a cylinder with a diameter of 20 mm and height of 450 mm, and V_s is the volume of the foam skeleton, which was determined by immersing the sample in a calibrated liquid measuring vessel. V_s was taken as the increase in liquid volume. For each of the foams, three samples were used to obtain measurements and the arithmetic mean of the results obtained was taken as the porosity.

Microscopic skeleton images were used to determine the size of cells and pores in the studied foams. The photographs were taken using an Inspekt F scanning microscope with 15× magnification. Foam images were analysed in Met-Ilo and Iris software.

Cell size d_c and pore size d_p were determined, as suggested by the authors of [33], as diameters of circles with the same circumferences as the cell and pore circumferences. The perimeter of the pore was traced along the edge of the skeleton. The length of the line running in the centre of the skeletal ligament forming a single cell was taken as cell perimeter (Figure 1).
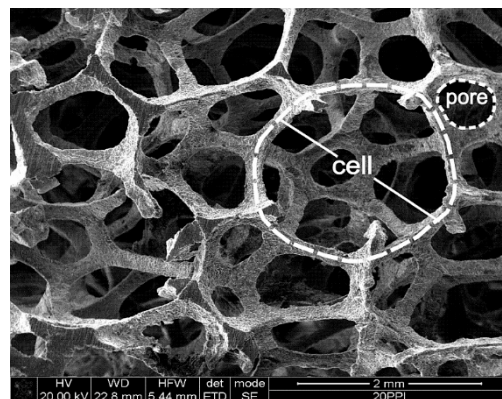

Figure 1. Example of a pore and a cell in a microscopic image of a 20 PPI foam skeleton.

More than 50 microscopic images were taken for each foam, allowing measurements of 104 cells of the 20 PPI foam, 159 cells of the 30 PPI foam and 185 cells of the 40PPI foam. The average sizes for each foam were taken as the cell diameter and pore.

2.1. Test Stand

The research was carried out using an experimental system, whose diagram is shown in Figure 2. A horizontal channel with an internal diameter of 20 mm and length of 2690 mm is the main element of this installation. The channel is filled with aluminium foam in the form of 30 mm long cylindrical inserts. An independent channel has been prepared for each foam. The channel is made of the aluminium pipe because the same system was used for heat transfer tests (their results are not discussed in this work). The 500 mm long end section of the channel has been made of colourless transparent Plexiglas, which allows observation of the gas–liquid flow patterns.

The pressure drop was measured in the middle of the channel as the difference in pressure between two points located 1000 mm apart. The first pressure measurement point was located at a distance of 1100 mm from the beginning of the channel. This distance was considered sufficient to get the flow fully stabilised. According to the authors of the [34,35] in single-phase flow through metal foams, the flow gets stabilised after a passage of 3–6 times the diameter of the foam cell. Information on the stabilization length for two-phase flow is missing from the literature. Authors of [6,13,14] conducted studies of gas–liquid flow through metal foams in channels with total length not exceeding fifty times the diameter.
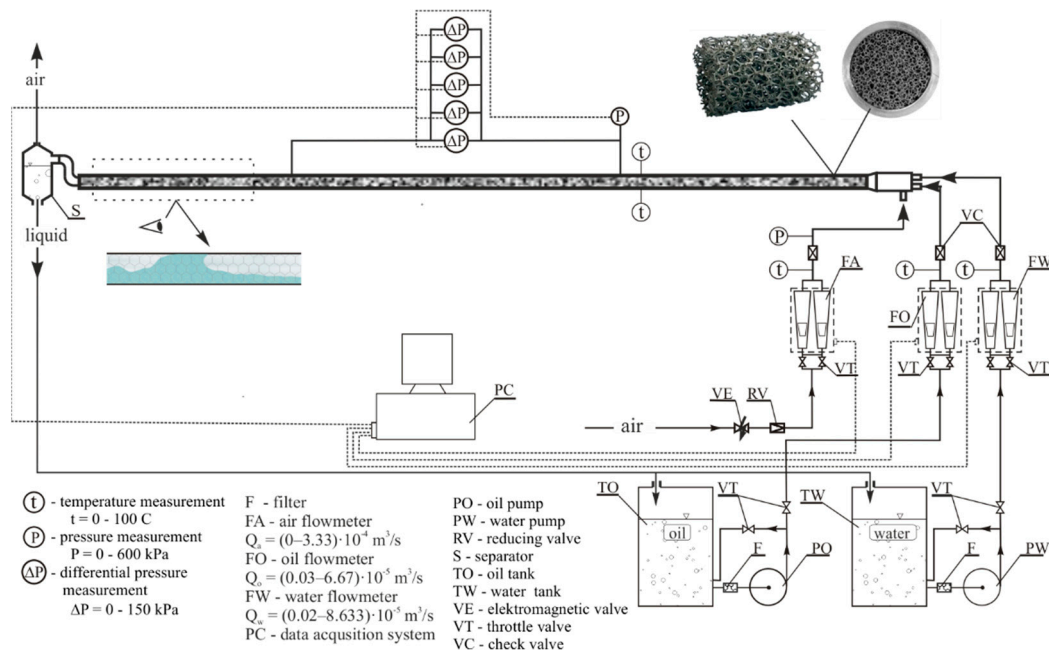
Figure 2. Diagram of the experimental stand used to single-phase and two-phase flow tests.

A set of five piezoresistive differential pressure sensors (Aplisens PR-28 and PR-50G) with a total measuring range of 0–150,000 Pa was used in the research. An additional piezoresistive sensor was used to measure the overpressure in the channel (relative to ambient pressure).

The air for testing was supplied from a pneumatic system [36]. Before air was introduced into the channel, its pressure was reduced to the desired level. The air flow rate was measured using two Kobold DMS mass flowmeters. Water was pumped using a multistage centrifugal pump and oil with a gear pump. Water flux was measured using two Kobold DPM turbine flowmeters. A Kobold KZA gear-wheel flowmeter was used to measure the oil flow rate. The air, water and oil flow rates were regulated using precision throttle valves.

The signals from all pressure and flow sensors were recorded using a computer data logging system developed in the DasyLab environment [37]. The characteristics of the measuring equipment are presented in Appendix A.

2.2. Research Methods

For all three foams, tests were carried out under the same flow conditions which were intended to determine the effect of foam structure on pressure drop and flow patterns. The fluid superficial velocity v_f, calculated with respect to the total channel cross-section, excluding foam and the second fluid (in two-phase flow), was adopted as the main quantity describing the flow conditions,

$$v_{sf} = Q_f \frac{4}{\pi d_k^2}, \ f = a, \ w, \ o \qquad (2)$$

where: Q_f—flow rate d_k—channel diameter.

The flow rates were set up to obtain flows in laminar and turbulent regimes and a wide range of changes in the void fraction in the gas–liquid flow. All basic flow patterns were expected to occur. It was supposed to enable the determination of their influence on pressure drop. The range of changes in the flow rate for specific phases was determined based on the results of previous research conducted by the author of this paper with te

use different metal foam [38]. Test conditions are presented in Table 5. The value of ε_f was determined according to the relation,

$$\varepsilon_f = \frac{Q_f}{Q_g + Q_l}. \tag{3}$$

Table 5. Range of experimental data.

Fluid, f	Single-Phase Flow		
	v_{sf}, m/s	g_f, kg/(m^2·s)	Re_f [1]
air, a	0.028–9.88	0.035–14.61	23–13244
water, w	0.003–0.270	2.78–270.14	30–4509
oil, o	0.003–0.167	2.39–143.42	3–293
	two-phase flow		
	v_{sf}, m/s	g_f, kg/(m^2·s)	ε_f −
air, a	0.028–2.39	0.035–2.89	0.313–0.998
water, w	0.006–0.061	5.69–61.49	0.002–0.988
oil, o	0.006–0.061	4.84–52.91	0.002–0.988

[1] Determined using Equation (6).

The flow characteristics were calculated for the average temperature and pressure measured in the channel. The temperature of the fluids during the tests was 22–24 °C.

Gas–liquid flow tests were carried out in series with a constant liquid flow rate and a gradually increasing air flow rate. Five values of water and oil flows were assumed. The air flow rate was increased in 19 steps. Once the flow rate stabilised, pressure drop was measured for 180 s. In this way, for each foam, the two-phase pressure drop was measured for 95 different conditions for both air–water flow and air–oil flow. Single-phase flow pressure drop measurements of each fluid were carried out in two series. In the first, the fluid flow rate was gradually increased and in the second, the fluid flow rate was decreased. Measurements were carried out for 33 different oil flow settings and over forty air and water flow settings.

Simultaneously with gas–liquid pressure drop measurements, we also observed flow patterns. The patterns were identified based on visual observations and the analysis of fluctuations in the measured pressure drop. An advanced algorithm was used in the analysis to classify flow patterns based on the fractal parameters of the differential pressure sensor signal. This methodology for identifying flow patterns was described in [39]. Four basic flow patterns were distinguished during the study: stratified, plug, slug and churn flow.

3. Results and Discussion

3.1. Pressure Drop in Single-Phase Gas and Liquid Flow

For all the tested flow cases (for all liquids and foams), the measured pressured drop in single-phase flow increases monotonically with increasing fluid velocity. Air and water pressure drop increases exponentially (Figures 3 and 4), and as shown in [40] can be described using Forchheimer law. Measurement uncertainties were not marked in the graphs showing the results of pressure drop measurements as due to the high accuracy of the measurements, the error bars coincide with the symbols of the measurement points.

For oil flow, the change in pressure drop is almost linear (Figure 5). Air and water pressure drop also change in a linear manner when their velocities are relatively low ($v_{sw} < 0.03$ m/s and $v_{sa} < 1$ m/s).

The linear dependence between pressure drop and fluid velocity is indicative of a laminar flow regime. With increasing velocity, the flow gradually changes to turbulent. For oil, the flow is laminar over the entire range of velocity changes. This is due to the fact that oil is several times more viscous than water.
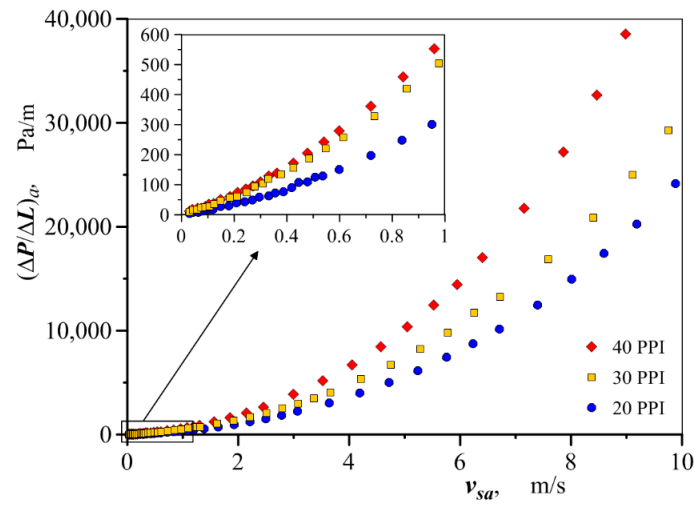
Figure 3. Change in measured pressure drop for air through metal foams as a function of air velocity.
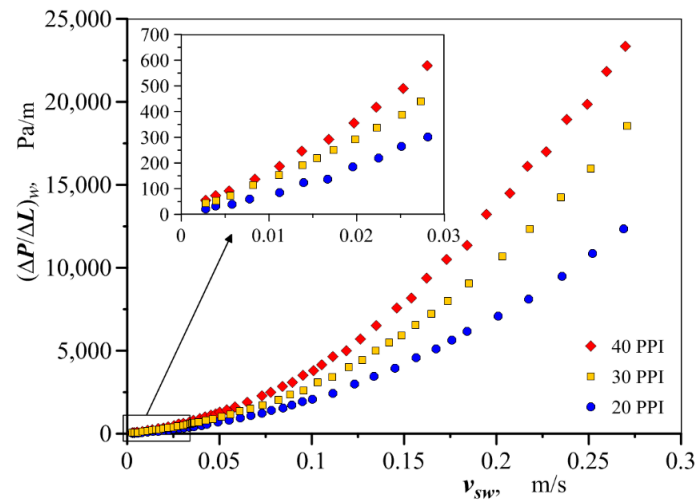

Figure 4. Change in measured pressure drop for water through metal foams as a function of the water velocity.
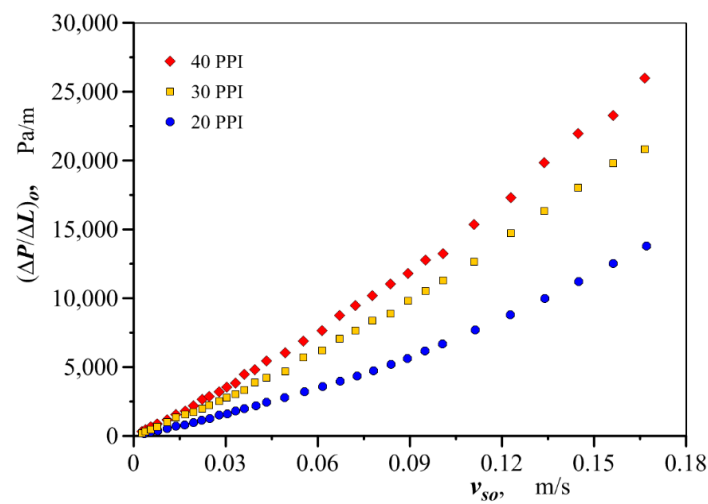

Figure 5. Change in measured pressure drop for oil through metal foams as a function of the oil velocity.

The laminar flow limit was determined by analysing changes in the friction factor f_{exp}, which was determined according to relation (4), based on the measured pressure drop $(\Delta P / \Delta L)_{exp}$ and the Darcy-Weisbach equation,

$$f_{exp} = \left(\frac{\Delta P}{\Delta L} \right)_{exp} \left(\frac{v_{sf}}{\phi} \right)^{-2} \frac{2d_e}{\rho_f}. \tag{4}$$

In Equation (4), there is a equivalent quantity d_e, defined based on two mutually independent geometrical parameters of the foam—porosity ϕ and pore diameter d_p that plays the role of hydraulic diameter.

$$d_e = \frac{\phi d_p}{1 - \phi}. \tag{5}$$

This takes into account the influence of the geometrical structure of the foam on the flow conditions, as expressed by the Reynolds number, described by the relation,

$$Re_f = \frac{v_{sf} d_e \rho_f}{\phi \mu_f}. \tag{6}$$

Information published in the literature, among others in [33,41] indicates that it is not possible to obtain flow similarity if the Reynolds number is defined based on channel size or foam permeability, as it is often done when describing flow through channels filled with metallic foams.

With the introduction of porosity to Equations (4) and (6), the friction factor and the Reynolds number are determined for the average fluid velocity, regardless of the type of foam which fills the channel.

For small Reynolds numbers, the friction factor decreases linearly (in a double logarithmic system) as *Re* increases. For all three fluids, a linear dependence between friction factor and the Reynolds number occurs when *Re* does not exceed a value of about 150 (Figure 6). This value is therefore the upper limit of laminar flow. For oil, laminar flow covered almost the entire range of tests carried out.
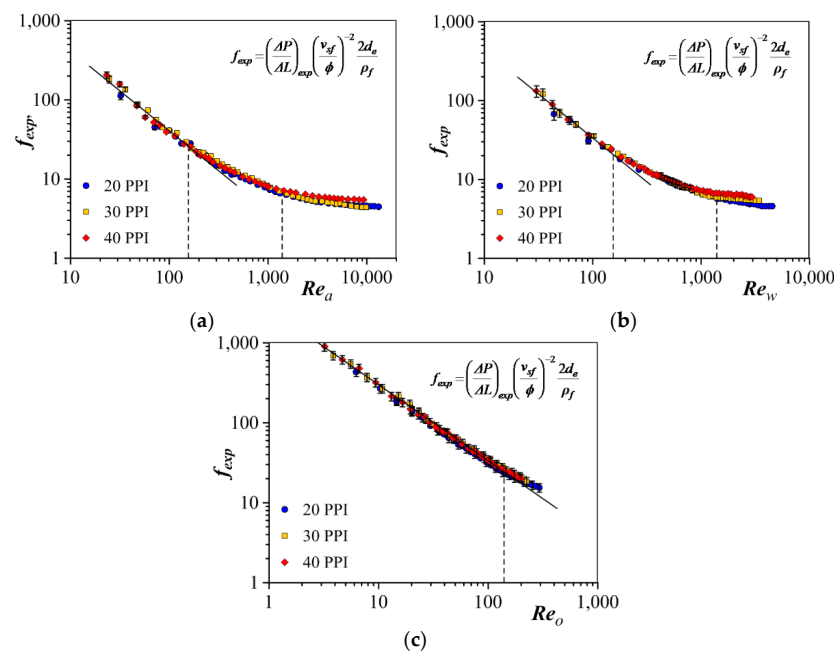
Figure 6. Change in the friction factor determined from measured pressure drop as a function of Reynolds number: (**a**) air flow; (**b**) water flow; (**c**) oil flow. (The uncertainty for friction factor was determined using Equation (A2)—Appendix A).

As the fluid velocity and the corresponding Reynolds number increase, the flow gradually takes on the characteristics of turbulent flow. It is evidenced by a clear deviation of the friction factor from a straight line when $Re > 150$. It is noticeable that when $Re < 1300$ the inclination of the friction factor curve is greater than when $Re > 1300$. When $Re \approx 150 \div 1300$ the flow takes the characteristics of Forchheimer transition flow. To the best of our current knowledge, in the Forchheimer regime deviations from laminarity are small. As the fluid velocity increases, the flow becomes increasingly unstable. When $Re > 1300$ the effect of fluid turbulence on the friction factor value is much smaller, at the same time the values of friction number determined for the flow through individual foams start diverging slightly. A similar situation was noted by Xu et al. [42] as well as Teruel and Rizwan-Uddin [43]. At a sufficiently high degree of turbulence, inertial forces dominate over viscous forces, which makes the influence of the geometrical structure of the foams on flow phenomena more salient. One can then speak of a Froud transition flow, i.e., a flow which, despite the lack of fully developed turbulence, can still be treated as a turbulent flow.

At the same fluid velocities, the highest pressure drop was recorded for flowing oil (Figure 7), i.e., the fluid with the highest viscosity. Pressure drop in water flow is 3 to 8 times lower than that of oil flowing at the same velocity. The greatest difference was found at low flow velocities when both fluids are laminar. As the fluid velocity increases, the water shows signs of turbulence and the drop in its pressure increases faster than for oil, which flowed laminar throughout the test range.
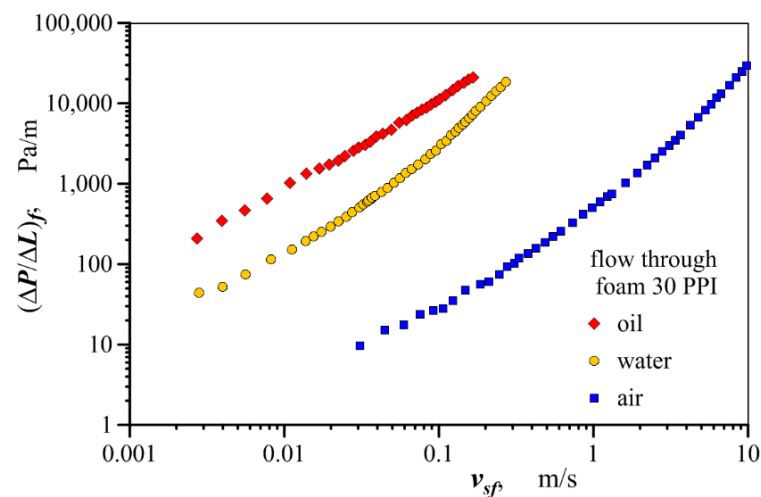
Figure 7. Measured pressure drop comparison for air, water and oil flowing through 30 PPI foam.

The results show a clear effect of the foam structure on the pressure drop. The lowest pressure drop was recorded when flowing through a 20 PPI foam and the highest when flowing through a 40 PPI foam, as can be seen in Figures 3–5. The 20 PPI foam has the largest cells and pores and therefore offers less resistance than foams with smaller cells.

The situation is less clear for the other two foams. The cell and pore size of 40 PPI foam is slightly larger than that of 30 PPI foam, yet the pressure drop in flow through 40 PPI foam is significantly higher than that of 30 PPI foam. The reason for the higher hydraulic pressure drop of 40 PPI foam seems to be its lower porosity and different geometrical structure (Figure 8). The cells of a 40 PPI foam are more "closed" due to large nodes connecting the skeleton fibres. Furthermore, in many places (Figure 8c) the skeleton of PPI foam is strongly deformed, which may cause a local increase in pressure drop.

3.2. Two-Phase Pressure Drop

Pressure drop in two-phase flow increases as the gas and liquid velocities increase. When the air velocity is in the range of 0–1 m/s the pressure drop is proportional to the air velocity, further increasing the air velocity results in a compounded increase in the pressure drop as can be seen in Figure 9. This figure shows the results of air–water flow

through 40 PPI foam, for the other foams the course of change in pressure drop in air–water flow is analogous. This nature of the change in pressure drop in both two-phase flow and single-phase flow is related to the change in flow regime. When the phase velocities are relatively low the gas–liquid mixture flows in a laminar manner. In single-phase flow studies, the liquid flow took on turbulent characteristics at twice the maximum liquid velocity in two-phase flow studies.
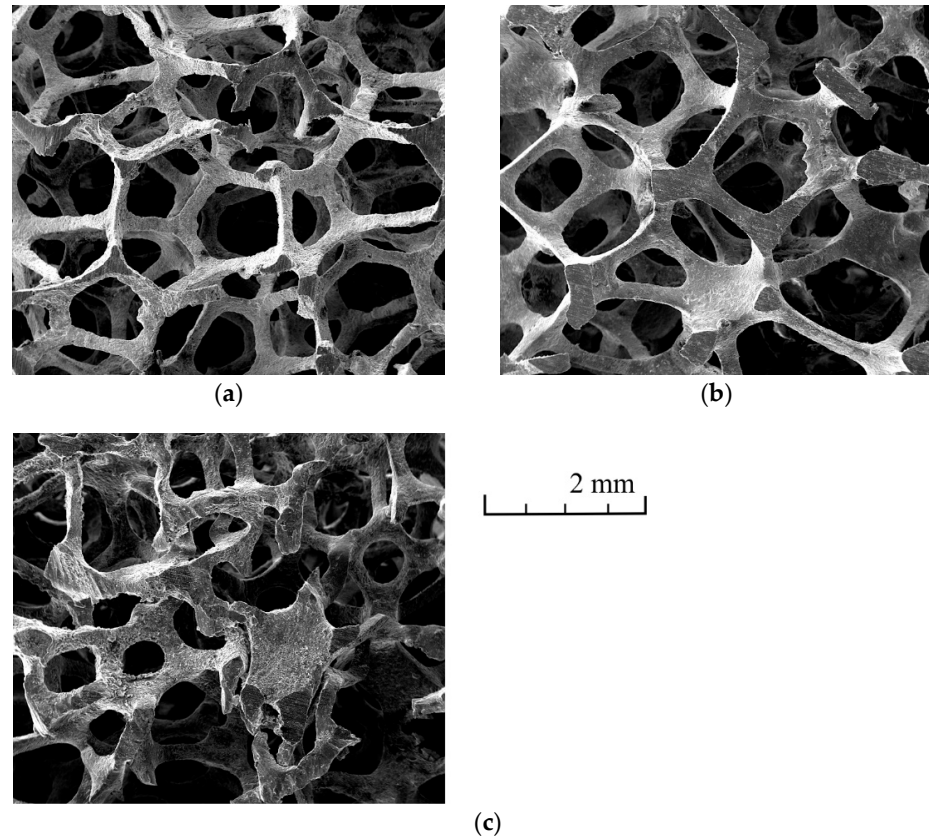

(**a**)

(**b**)

(**c**)

Figure 8. Cellular skeleton of foams used in this research: (**a**) 30 PPI foam; (**b**) 40 PPI foam; (**c**) local deformation of the cellular skeleton of 40 PPI foam.
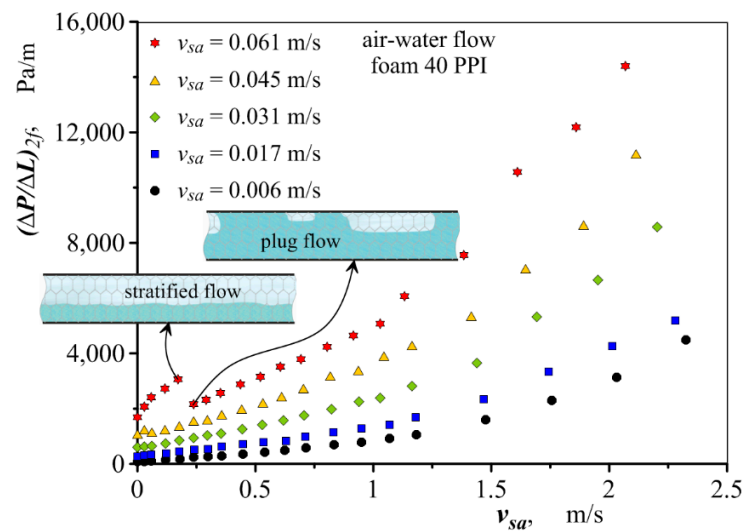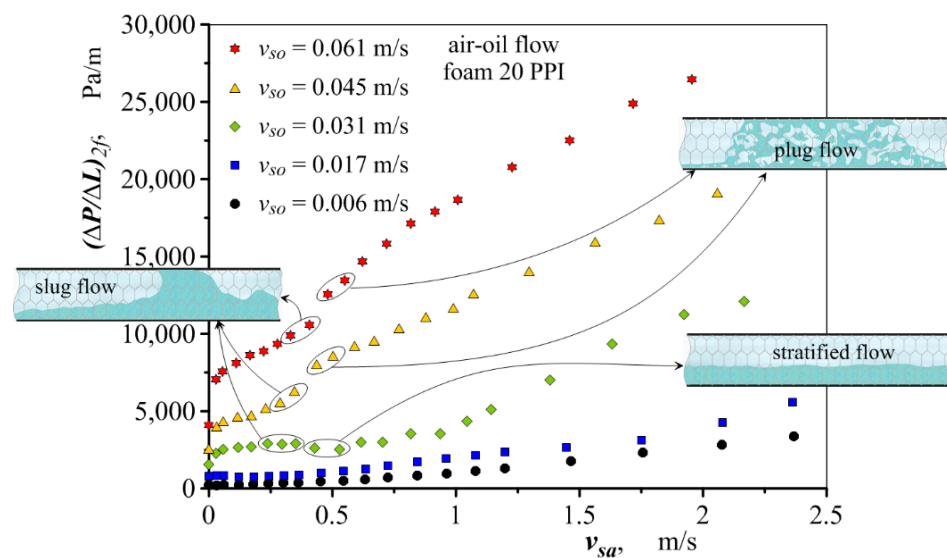

Figure 9. Measured pressure drop in the air–water flow as a function of the phase velocity (flow through 40 PPI foam channel)

The power character of pressure drop in air–water flow changes is more clearly visible when the air velocity exceeds approx. 1.0–1.2 m/s, which corresponds to the velocity at which the single-phase air flow ceases to be laminar.

The only deviation from the monotonic increase in pressure drop in air–water flow is the abrupt decrease in pressure drop in two-phase flow recorded for a flow with a water velocity of 0.061 m/s when the air velocity increases from 0.2 to 0.24 m/s. Under these conditions plug flow changes to stratified flow. The reduction in the pressure drop results from a reduction in the contact area between the water and the foam skeleton. As a more viscous phase, water determines the value of pressure drop in two-phase flow to a greater extent than air. In plug flow, the water wets almost the entire surface of the channel and the foam. In stratified flow, water usually occupies less than half of the channel cross-section. Reduction in pressure drop is typical of multiphase flows [44,45], however, they have not yet been described in papers on flow through open-cell foams.

Pressure drop in air–oil flow also shows an increasing trend with increasing phase velocity (Figure 10). However, the pressure drop curves are more varied than for air–water flow, due to the greater variety of flow patterns observed in air–oil tests.

Figure 10. Measured pressure drop in air–oil flow as a function of phase velocity (flow through 20 PPI foam channel).

In air–water flow tests, the stratified flow was the dominant flow type, accounting for more than 70% of all flow cases. In studies of air–oil flow, slug flow and churn flow were frequently observed under conditions where the stratified flow was present in the air–water flow. In studies involving oil, plug, slug and churn flows accounted for more than 50% of the flow cases studied. The energy lost to form the interfacial surface varies across the individual flow patterns, which in combination with the different degree of foam wetting by the fluid manifests itself in a non-uniform course of changes in pressure drop in the gas–liquid flow. These situations are illustrated in Figure 10 (measurement series v_{so} = 0.031 m/s).

At equal phase velocities, the measured pressure drops in air–oil flow are clearly higher than for air–water flow. Similarly, as in single-phase flow, the lowest pressure drop in two-phase flow was recorded in the flow through a channel filled with 20 PPI foam, whereas the highest in flow through 40 PPI foam.

4. Modelling Pressure Drop

In the search for a method of predicting pressure drop in gas–liquid flow in channels filled with metal foams, first checked was the possibility of using models describing pressure drop in boiling liquid in evaporators filled with metal foam. For this purpose, the meth-

ods proposed by the authors of papers [11,13,14,23,25,27,29] were selected. The model developed by Tourvieille et al. [23] for flow through mini-channels filled with foam was also taken into account. Table 6 summarises the correlations included in the analysed computational models. Figure 11 compares the measured pressure drops in air–water and air–oil flows with the corresponding values calculated using the correlations in Table 6.

Table 6. Correlations describing the pressure drop of gas–liquid flow in channels with metal foam packing.

Authors	Main Correlations	Other Correlations	$\delta(\Delta P)$ [1]
Bamorovat Abadi et al. [27]	$\left(\frac{\Delta P}{\Delta L}\right)_{2f} = \left(\frac{\Delta P}{\Delta L}\right)_{2f,Empty}\varphi_l^2$ $\left(\frac{\Delta P}{\Delta L}\right)_{2f,Empty} = f\frac{2g_{sl}^2}{\rho_{2f}d_h}$	$C = PPI^{0.03}g_{2f}^{0.45}e^{-1.7x}$ $f = \frac{16}{Re_{2f}}$ if $Re_{2f} < 2000$	71.5
Gao et al. [25]	$\left(\frac{\Delta P}{\Delta L}\right)_{2f} = \int_{x_{in}}^{x_{out}} f\frac{g_{2f}^2}{d_h\rho_{2f}}dx$	$f_l = 0.2316Re^{-0.31}$	96.0
Hu et al. [13]	$\left(\frac{\Delta P}{\Delta L}\right)_{2f} = \left(\frac{\Delta P}{\Delta L}\right)_l\varphi_l^2$ $\left(\frac{\Delta P}{\Delta L}\right)_l = \frac{a(1-\phi)^2a_{mf}^2\mu_l v_{sl}}{\phi^3} + \frac{b(1-\varepsilon)a_{mf}\rho_l v_{sl}^2}{\phi^3}$	$C = 27.268g_{2f}^{-0.38}e^{-0.477x}d_p^{-0.181}e^{0.149\times100\omega}$	193.5
Ji and Xu [14]	$\left(\frac{\Delta P}{\Delta L}\right)_{2f} = \left(\frac{\Delta P}{\Delta L}\right)_l\varphi_l^2$ $\left(\frac{\Delta P}{\Delta L}\right)_l = \int_0^{x_{out}} \frac{f_l g^2(1-x)^2 v_l(1-\phi)}{d_h\phi^3}dx$	$f_l = 55980\frac{(1-\varphi)}{Re^{1.19}}d_p^{0.94} + 0.22$ $C = 0.025g_{2f}^{1.801}e^{8.021x}d_p^{0.455}$	210.6
Shi et al. [11]	$\left(\frac{\Delta P}{\Delta L}\right)_{2f} = \left(\frac{\Delta P}{\Delta L}\right)_l\varphi_l^2$ $\left(\frac{\Delta P}{\Delta L}\right)_l = \frac{a(1-\phi)^2a_{mf}^2\mu_l v_{sl}}{\phi^3} + \frac{b(1-\varepsilon)a_{mf}\rho_l v_{sl}^2}{\phi^3}$	$C = -1.6819G_g^{-1.0787}e^{-0.0146x}d_c^{1.7645}$	68.2
Tourvieille et al. [23]	$\left(\frac{\Delta P}{\Delta L}\right)_{2f} = \left(\frac{\Delta P}{\Delta L}\right)_l\varphi_l^2$ $\left(\frac{\Delta P}{\Delta L}\right)_l = \left[\left(\frac{\Delta P}{\Delta L}\right)_{l,Empty} + \left(\frac{\Delta P}{\Delta L}\right)_{l,mf}\right]$ $\left(\frac{\Delta P}{\Delta L}\right)_{l,Empty} = f\frac{v_{sl}^2}{2d_h}\rho_l \left(\frac{\Delta P}{\Delta L}\right)_{l.mf} = \frac{\mu_l}{K}v_{sl}$	$fRe_l = \frac{6}{\left[1 - \frac{192}{\pi^5}tanh\left(\frac{\pi}{2}\right)\right]}$ $C = 5$	44.9
Weise et al. [29]	$\left(\frac{\Delta P}{\Delta L}\right)_{2f} \approx \beta\frac{1}{\rho_{2f}}g_{2f}$	β—Forchheimer coefficient	128.5
Correlations common for the models [11,13,14,23,27]. $\varphi_l^2 = 1 + \frac{C}{X} + \frac{1}{X^2}$; $X = \left(\frac{1-x}{x}\right)^{0.5}\left(\frac{\rho_g}{\rho_l}\right)^{0.5}\left(\frac{\mu_l}{\mu_g}\right)^{0.5}$			
$a_{mf} = 4.867\frac{1-0.971(1-\varphi)^{0.5}}{d_p(1-\varphi)^{0.5}}$; $a = \left[\frac{\varphi\left(1-0.971(1-\varphi)^{0.5}\right)}{0.6164(1-\varphi)^{0.5}}\right]^{-1}$; $b = \frac{(1-\varphi)\left(1-0.971(1-\varphi)^{0.5}\right)}{0.6164(1-\phi)^{0.5}}$			
$\frac{1}{\rho_{2f}} = \frac{x}{\rho_g} + \frac{1-x}{\rho_l}$; $\mu_{2f} = x\mu_g + (1-x)\mu_l$			

[1] $\delta(\Delta P)$—mean absolute error calculated in relation to the experimental pressure drop from present study.
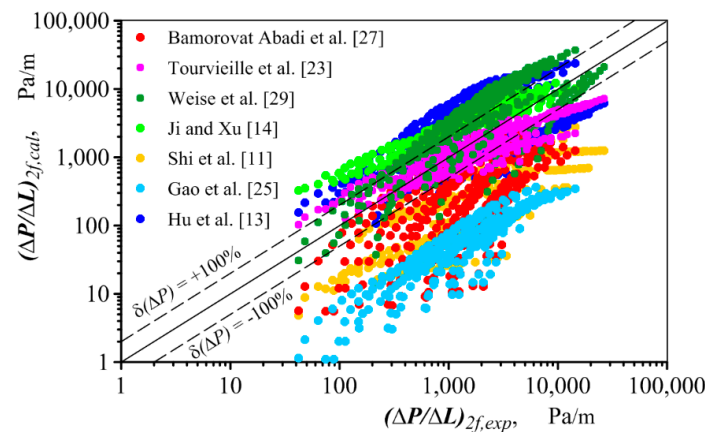

Figure 11. Comparison between measured pressure drops in gas–liquid flow $(\Delta P/\Delta L)_{2f,sxp}$ and pressure drops $(\Delta P/\Delta L)_{2f,cal}$ calculated from the correlations proposed by references [11,13,14,23,25,27,29].

The calculated pressure drops differ very significantly from the measured pressure drops. For the model developed by Hu et al. [13] the mean calculation error (ratio of the difference between the calculated and measured pressure drop to the measured value) is more than 193% and for the Ji and Xu method, it exceeds 210% (Table 6). For other models, the errors are smaller but still too large to be considered satisfactory.

The intended use of the analysed models should certainly be cited among the reasons for such large discrepancies. Except for the model of Tourvieille et al. [23], all these models were developed to predict pressure drop in boiling refrigerants, a process in which pressure drop is largely determined by factors not present in gas–liquid flow without a change of state of aggregation. For example, Ji and Xu [14] found that the pressure drop during boiling is higher than in gas–liquid flow without boiling, and they pointed to vapour bubbles blocking foam cells adjacent to the channel wall during nucleation as the cause. Similar observations were made by Gao et al. [25]. Furthermore, the authors of [14] showed that pressure drop in a boiling mixture depends on heat flux. The influence of heat flux on the hydrodynamics of flow through metal foams was also reported by Li et al. [5]. The models describing pressure drop in boiling liquid were developed based on tests conducted at much higher mass flux than the pressure drop measurements reported in this paper ($g_{2f} < 64 \text{ kg·m}^{-2}\text{·s}^{-1}$), which may also be the cause of significant calculation errors. Boiling in flow is usually investigated at mass fluxes of tens to hundreds of kg·m^{-2}·s^{-1}.

The best results were obtained with the model by Tourvieille et al. [23], which is the only one developed based on gas–liquid flow tests without boiling or condensation. For the model of Tourvieille et al., the average calculation error is less than 45%. Please note, however, that despite the statistically good fit between calculated and measured pressure drops, for some data points the calculated values are up to 3 times higher (for small mass flux) or lower (for large mass flux) than the measured values. Furthermore, as illustrated in Figure 12, the calculated pressure drop is boosted by increasing gas velocity to a lesser extent than the measured resistance.
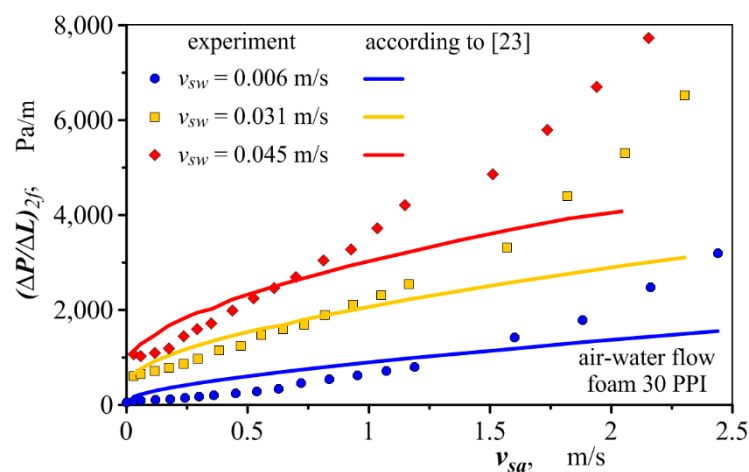
Figure 12. Comparison of changes in the pressure drop value measured and calculated with the use of the model [23] as a function of the air velocity for selected conditions of the air—-water flow through a channel filled with 30 PPI foam.

Tourvieille et al. [23] developed their flow resistance model based on tests conducted for laminar flow with liquid velocities not exceeding 0.025 m/s and gas velocities up to 0.06 m/s. The studies described in this paper were carried out for phase velocities greatly exceeding these values, which may be the reason for the different nature of the pressure drop changes, especially at high gas velocities.

Since the analysed pressure drop models include no one that correctly reflects the value and nature of pressure drop changes in gas–liquid flow through metal foams, a decision was made to develop a new model to predict this value.

The performed observations of the flow patterns show that the foam does not disperse the fluids in the channel. In all two-phase flow cases, gas and liquid were clearly separated. Therefore, we assumed that the pressure drop in two-phase flow through foam-filled channels could be calculated using a separated flow model, based on a pressure drop in a single-phase flow of liquid and gas.

Fluid pressure drop $(\Delta P / \Delta L)_l$ could be determined using the Darcy-Weisbach equation,

$$\left(\frac{\Delta P}{\Delta L}\right)_l = f \frac{v_{sl}^2}{2\phi^2} \rho_f \frac{1}{d_e}. \tag{7}$$

Relatively high pressure drops in the flow through metal foams, of the order of tens of thousands Pa/m, can cause significant changes in gas density. Among others, Azzi et al. [46] and Dhiman et al. [47] pointed to this issue. To take into account the influence of the gas compressibility on the value of pressure drops in the gas flow, we propose to calculate this quantity based on the pressure changes along the flow path (P_1 and P_2), using the equation

$$\left(\frac{P_1^2 - P_2^2}{\Delta L}\right)_g = f \frac{m_g^2}{A^2 \phi^2} R_g T_g \frac{1}{d_e}. \tag{8}$$

where: m_g—gas mass flow rate, A—area cross-sectional of the channel, R_g—specific gas constant, T_g—temperature absolute.

The pressure drop in flow through metal foams is determined by phenomena occurring at the level of individual cells and skeletal fibres. Therefore, we assumed that in calculating pressure drop, an equivalent diameter Equation (5), which captures the structural parameters of the foam, should play the role of the hydraulic diameter.

The friction factor, which appears in Equations (7) and (8), must be defined appropriately for flow through metal foams. Figure 13 collects the friction factor values for all flow cases. The way the Reynolds number and equivalent diameter are defined (Equations (5) and (6)) ensures that for the same flow conditions the friction factor has a similar value regardless of the type of fluid and foam through which it flows. This makes it possible to describe the friction factor with a relation common to all fluids and foams.
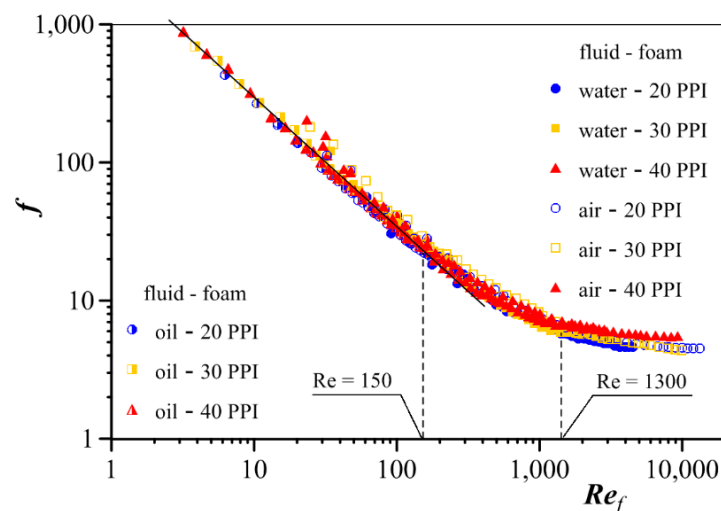

Figure 13. Friction factor for all single-phase flow cases tested.

Separate formulas describing the friction factor were adopted for the different flow regimes:

$$f = 2260 Re_f^{-0.9}, \text{ for } Re_f < 150, \tag{9}$$

$$f = 103 Re_f^{-0.4} + 12530 Re_f^{-1.4}, \text{ for } Re_f = 150\text{--}1300, \tag{10}$$

$$f = 37 \text{Re}_f^{-0.14} \left(\frac{\phi d_p}{d_c - d_p} \right), \text{ for } Re_f > 1300. \tag{11}$$

Equations (9) and (10) are typical for flow through porous media. In the Froud regime, the influence of foam morphology on the flow hydrodynamics becomes evident; therefore, Equation (11) includes a term that accounts for the geometrical parameters of foam—ϕ, d_p and d_c.

The average error in pressure drop in single-phase flow calculated using the set of Equations (7)–(11) is 9.3%, and 95% of the calculation results have an error smaller than $\pm 15\%$ (Figure 14).
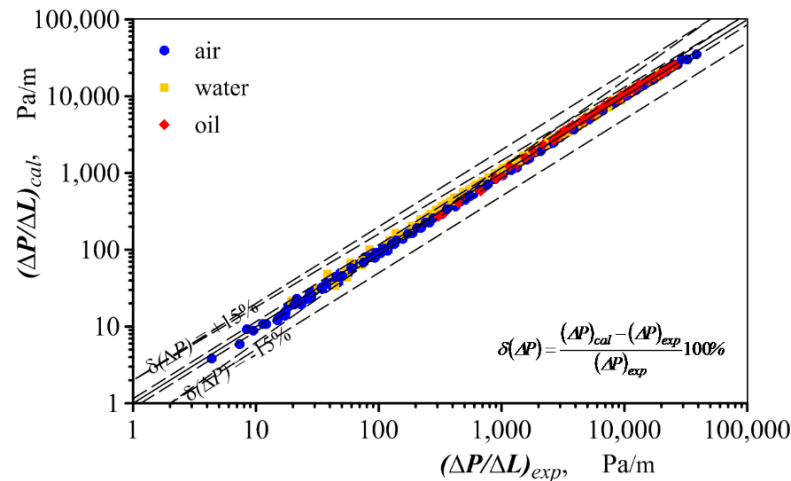
Figure 14. Comparison between the measured pressure drops in the single-phase flow and pressure drops calculated from Equations (7) and (8).
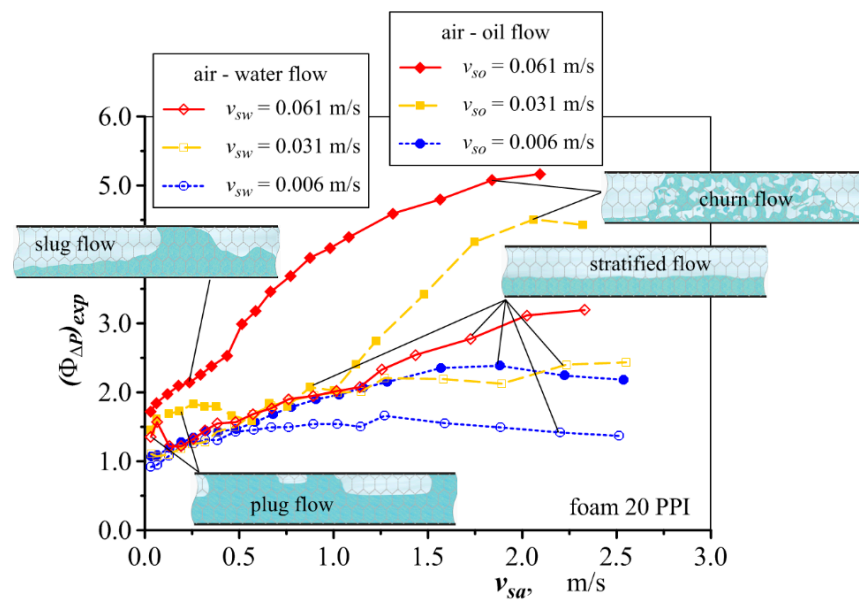
Measurement results indicate that the pressure drop in gas–liquid flow is usually higher than the sum of pressure drop in single-phase gas and liquid flowing at the same velocities as in two-phase flow. Therefore, we assumed that pressure drop in gas–liquid flow can be described by the relation,

$$\left(\frac{\Delta P}{\Delta L} \right)_{2f} = \left[\left(\frac{\Delta P}{\Delta L} \right)_l + \left(\frac{\Delta P}{\Delta L} \right)_g \right] \Phi_{\Delta P} \tag{12}$$

in which the parameter $\Phi_{\Delta P}$ is a measure of pressure drop amplification in double-phase flow compare to the sum of pressure drops in gas and liquid single-phase flows.

Initially, the pressure drop amplification factor $\Phi_{\Delta P}$ was determined based on measured pressure drops in single-phase and two-phase flows. The data obtained indicate that the value of the pressure drop amplification factor depends on several factors. One of these includes fluid velocity. In two-phase flow, an increase in velocity causes a more intensive interaction between liquid and gas, which results in a greater dispersion of energy than in single-phase flow (for the same increase in velocity).

For this reason, the increase in pressure drop in single-phase gas–liquid flows does not correspond to a change in pressure drop in gas–liquid flow, and the pressure amplification factor takes a value greater than 1 (Figure 15). The friction factor only takes the value smaller than 1 in the few cases where there is a reduction in pressure drop in two-phase flow, associated with changes in flow patterns. Figure 15 only presents selected representative data to ensure the legibility of the graph. The pressure drop amplification factor value for air–oil flow is higher than for air–water flow. This proves that the fluid properties must be taken into account in the mathematical description of the amplification factor.

Figure 15. Changes in the pressure drop amplification factor (values obtained from measured pressure drops).

The analysis of correlation calculations and the significance test of various factors indicate that the amplification factor can be described by the equation,

$$\Phi_{\Delta P} = 1 + C Re_l^{c_1} Re_g^n \left[\left(\frac{\eta_l}{\eta_w} \right) \left(\frac{\rho_w}{\rho_l} \right)^2 \right]^{c_2}. \tag{13}$$

The influence of the velocity and physical properties of the fluids on the amplification factor has been captured by Reynolds numbers. The importance of fluid viscosity and density is so great that it was necessary to introduce an additional term in Equation (13) to capture these properties.

The exponent n at the Re_g number is a measure of the fluid-gas interaction, and was described using quantities characterising fluid flow—the friction factor f_l and the Darcy number Da_l,

$$n = D \left(1 - \frac{1}{f_l} \right)^{-1} \log Y_{gl}^{b_1} + B Da_l^{b_2}, \tag{14}$$

where: f_l is determined in line with Equation (9), (10) or (11).

The Darcy number is described by the equation,

$$Da_l = \frac{K}{(0.5 d_k)^2}, \tag{15}$$

in which K is the foam permeability.

The Y_{gl} parameter is described with the equation,

$$Y_{gl} = \frac{\left(\frac{\Delta P}{\Delta L} \right)_l}{\left(\frac{\Delta P}{\Delta L} \right)_{gl}}, \tag{16}$$

where: $(\Delta P / \Delta L)_{gl}$ expresses pressure drop in gas flowing with a velocity equal to liquid velocity.

As mentioned earlier, the pressure drop in stratified flow is significantly lower than that of plug, slug and churn flows, which manifests itself in the discontinuity of the pressure drop curve when stratified flow changes into another type of flow (or vice versa). There-

fore, the values of constants and exponents in Equations (13) and (14) were determined separately for stratified and other flows. For stratified flow:

$$C = 0.0001; c_1 = 0.2; c_2 = 0.33; D = 0.33; B = 0.125; b_1 = 0.25; b_2 = -0.25;$$

for plug. slug and churn flows.

$$C = 0.0018; c_1 = 0.45; c_2 = 0.66; D = 0.11; B = 0.07; b_1 = 0.5; b_2 = -0.25;$$

The type of flow pattern can be determined using the flow map shown in Figure 16 that we developed in [48].
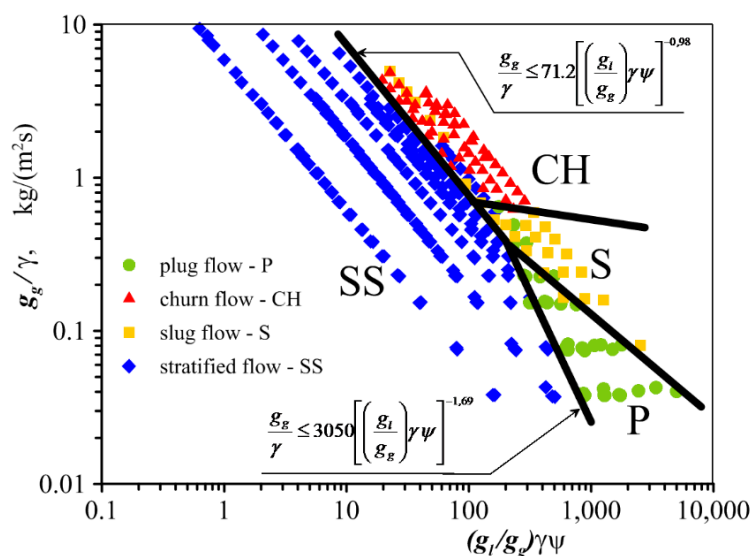

Figure 16. Map of the gas–liquid flow through horizontal channels filled with metal foams, developed by Dyga and Placzek [48].

According to this map, stratified flow occurs when the following conditions are met:

$$\begin{cases} \frac{g_g}{\gamma} \leq 71.2\left[\left(\frac{g_l}{g_g}\right)\gamma\psi\right]^{-0.98} & dla \left(\frac{g_l}{g_g}\right)\gamma\psi = 1 \div 200 \\ \frac{g_g}{\gamma} \leq 3050\left[\left(\frac{g_l}{g_g}\right)\gamma\psi\right]^{-1.69} & dla \left(\frac{g_l}{g_g}\right)\gamma\psi > 200 \end{cases} \tag{17}$$

where: g—mass flux

Dimensionless parameters γ and ψ describe equations,

$$\gamma = \left[\left(\frac{\rho_g}{\rho_a}\right)\left(\frac{\rho_l}{\rho_w}\right)\right]^{0.5} \tag{18}$$

$$\psi = \left(\frac{\sigma_w}{\sigma_l}\right)\left[\left(\frac{\mu_l}{\mu_w}\right)\left(\frac{\rho_w}{\rho_l}\right)^2\right]^{1/3}, \tag{19}$$

where: σ—surface tension.

The results obtained based on Equation (12) and the complementary relationships reflect well the value and course of change in pressure drop in two-phase flow, as illustrated in Figures 17 and 18, for selected air–water and air–oil flow conditions. Figure 19 presents a comparison of all measured and calculated pressure drops. The statistical analysis shows that 82% of calculation results for pressure drop in two-phase flow have an error of less than ±25%.
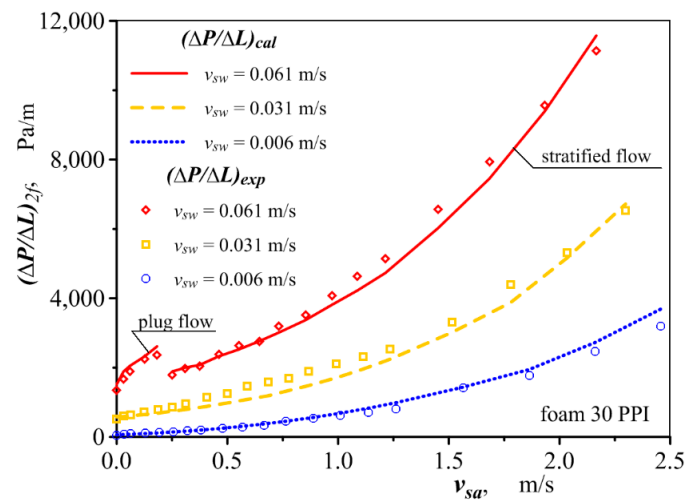
Figure 17. Pressure drop changes in the air–water flow calculated with the developed pressure drop model.
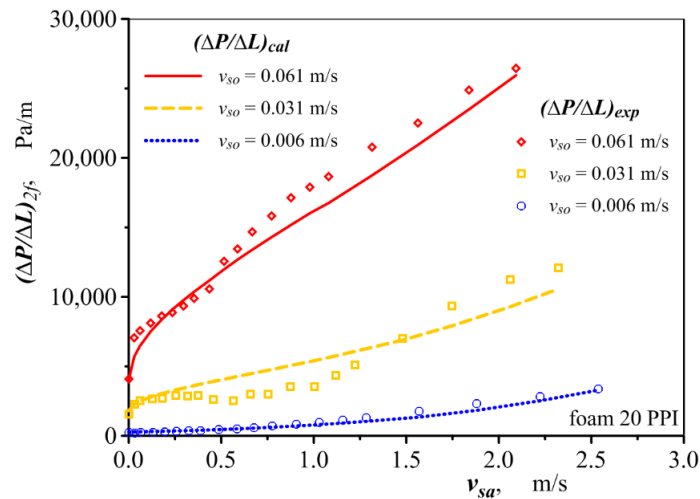
Figure 18. Pressure drop changes in the air–oil flow calculated with the developed pressure drop model.
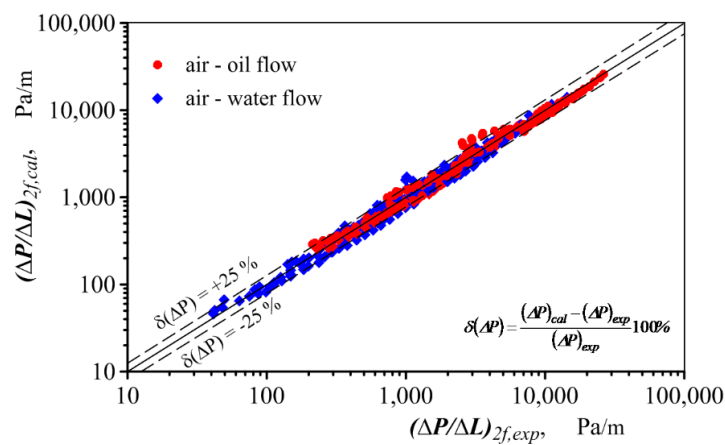
Figure 19. Comparison between the measured pressure drops in the gas–liquid flow $(\Delta P/\Delta L)_{2f,sxp}$ and pressure drops $(\Delta P/\Delta L)_{2f,cal}$ calculated from the Equation (12).

The developed computational model ensures that pressure drop in two-phase flow coincides with the pressure drop in single-phase flow when a gas or liquid disappears

in the flow. When the flux of one of the fluids approaches zero the Reynolds number approaches zero and, consequently $\Phi_{\Delta P}$ approaches 1.

5. Conclusions

The experimental investigations described in this paper were carried out with three fluids and three foams of different geometrical structure. The measurements were carried out across a relatively wide range of fluid velocity changes. A total of 936 results of pressure drop measurements were obtained for various hydrodynamic conditions in one-phase and two-phase flow (570 for gas–liquid flow). The analysis of our results and information from the literature allows us to formulate the conclusions presented below.

Metal foams have a very high porosity and completely open cells, which causes laminarization of the flow to a lesser extent than other porous materials. In addition to laminar flow, we can distinguish Forchheimer transition flow, which is characterised by a low degree of turbulence, and Froud transition flow. Froud flow bears the characteristics of turbulent flow.

The hydrodynamic similarity for flows through foams with different geometrical structure can be determined by the Reynolds number (Equation (6)), in which the role of the hydraulic diameter is played by the equivalent diameter (Equation (5)) defined based on the geometrical foam parameters. In this approach, the flow is laminar when $Re_f < 150$. In the $Re_f = 150$–1300 range, Forchheimer transition flow occurs, and when $Re_f > 1300$, Froud flow occurs.

Foam does not cause phase dispersion of the gas–liquid mixture. When flowing through channels filled with metal foams, homogeneous mixtures typical for flows through other porous media are not observed. In the course of our study, split flows typical of flows through hollow channels were observed.

The value of pressure drop is significantly influenced by the geometrical structure of the foam. The pressure drop increases with the decreasing cell diameter and porosity. For foams of similar cell size (2.25 mm and 2.38 mm), a decrease in porosity by less than 1.5% results in an increase in pressure drop by 28% on average. For the largest air streams, this difference reaches 50%. However, a higher pressure drop in the flow through the foam with lower porosity may also be related to differences in the skeleton shape.

For two-phase flow, flow patterns have a significant influence on pressure drop. Changes in flow patterns can be accompanied by step changes in pressure drop. This is most evident when changing from plug flow to stratified flow. A reduction in pressure drop is observed then despite an increase in flow velocity. The stratified flow is also characterised by pressure drop lower than the slug and churn flows.

Pressure drop in single-phase fluid flow can be determined based on the Darcy-Weisbach equation (Equation (7)) and the friction factor defined for flow through foam by Equations (9)–(11).

We have shown that pressure drop in two-phase flow can be determined as the sum of pressure drop in single-phase gas and liquid flow multiplied by the drop amplification factor (Equation (12)). The amplification factor depends on many factors. It is described by Equation (13) together with Equations (14)–(16).

Equations (12)–(16) form a model of pressure drop in gas–liquid flow through a channel filled with metallic foam. The model can be applied independently of the forming flow patterns. The values of some empirical constants were determined separately for stratified flow and other flow types, which made it possible to capture rapid changes in pressure drop under changing flow patterns.

The developed pressure drop model allows us to determine this quantity with satisfactory accuracy. For single-phase flow, 95% of the results have an error of less than 15%. For gas–liquid flow, 82% of the calculation results have an error smaller than 25%. The model can be applied to flow through horizontal channels filled with metal foams with a structure similar to that of the foams used in this study. The hydrodynamic conditions for the application of the proposed calculation methods shall be as given in Table 3. The pos-

sibility of calculating pressure drops over a wider range of changes in hydrodynamic conditions need to be verified.

Author Contributions: Conceptualization R.D.; methodology R.D. and S.B.; validation R.D.; formal analysis R.D.; investigation R.D.; software S.B.; data curation R.D. and S.B.; writing—original draft preparation R.D.; visualization R.D.; writing—review and editing R.D. and S.B. All authors have read and agreed to the published version of the manuscript.

Institutional Review Board Statement: Not applicable.

Informed Consent Statement: Not applicable.

Conflicts of Interest: The authors declare no conflict of interest.

Nomenclature

d	diameter, m
d_e	equivalent diameter acc. Equation (5), m
f	friction factor, –
g	mass flux, kg/(m^2·s)
G	mass flow rate, kg/s
PPI	pore density of metal foam (pore per inch)
Re	Reynolds number acc. Equation (6), –
Q	volumetric flow rate, m^3/s
v_s	superficial velocity, m/s
X	Martinelli parameter, –

Greek symbols

$\frac{\Delta P}{\Delta L}$	pressure drop, Pa/m
ϕ	porosity of foam, –
ϕ_l^2	two-phase frictional multiplier, –
$\Phi_{\Delta P}$	amplification factor acc. Equation (13), –
μ	dynamic viscosity, Pa·s
ε	volume fraction, –
ρ	density, kg/m^3

Subscripts

a	air
c	*cell*
cal	calculated
exp	experimental
f	phase, fluid
g	gas
l	liquid
o	*oil*
p	pore
w	water
2f	two-phase flow

Appendix A

The experimental results were evaluated in terms of measurement uncertainties [49]. The uncertainty analysis was conducted in accordance with the International Standards Organisation (ISO) Guide to the Expression of Uncertainty in Measurement [50]. The standard uncertainty of a parameter x, measured directly, is described by the formula,

$$u(x) = \sqrt{\frac{\Delta_d x^2 + \Delta_e x^2}{3}}. \tag{A1}$$

The calibration uncertainty dx of pressure sensors and air and water flow meters was determined based on their accuracy class, confirmed by calibration certificates. Due to its wide measuring range, the oil meter was calibrated using the weight method. The uncertainty for the oil flowmeter was determined using linear regression of the calibration results.

The experimenter's uncertainty $\Delta_e x$ was taken as the unit value of the last significant place displayed in the result recording system [51]. Table A1 presents the maximum values of the relative uncertainty of the individual measuring sensors. Relative uncertainty is the ratio of the standard uncertainty to the measured value.

Table A1. Uncertainties of the measured parameters.

Parameters	Instrument	Measurement Range	Accuracy *	Relative Uncertainty **
	Aplisens PR-50G	0–500 Pa	0.16%	1,5%
	Aplisens PR-28	500–2000 Pa	1.6%	3.7%
Differential pressure	Aplisens PR-28	2–10 kPa	0.40%	1.2%
	Aplisens PR-28	10–50 kPa	0.25%	0.7%
	Aplisens PR-28	50–150 kPa	0.25%	0.4%
Pressure	Aplisens PC-28	0–600 kPa	0.25%	0.3%
Air flow rate	Kobold DMS 1-11C4FD2	$0\text{–}3.33 \cdot 10^{-4} \text{ m}^3/\text{s}$	0.2%	2,4%
	Kobold DMS 2-14C4FD2	$3.33 \cdot 10^{-4}\text{–}3.33 \cdot 10^{-3} \text{ m}^3/\text{s}$	0.3%	1.7%
Water flow rate	Kobold DPM 1107G2L	$2.5 \cdot 10^{-7}\text{–}1.17 \cdot 10^{-5} \text{ m}^3/\text{s}$	1%	4.1%
	Kobold DPM1550G2L	$8.33 \cdot 10^{-6}\text{–}8.33 \cdot 10^{-5} \text{ m}^3/\text{s}$	1%	4.2%
Oil flow rate	Kobold KZA 1804R08	$3.33 \cdot 10^{-7}\text{–}6.67 \cdot 10^{-5} \text{ m}^3/\text{s}$	2%	6%
Temperature	K-type thermocouples	0–100 °C	0.1 K	0.9%

* Declared by the producer in relation to the measuring range. ** Refers to the measured value.

The friction factor was determined indirectly based on direct measurements of other quantities. Therefore, the friction factor uncertainty δf was determined by transferring uncertainties for direct measurements $u(x)$, using,

$$\delta f = \sqrt{\sum_{i=1}^{k} \left(\frac{\partial f}{\partial x_i} \right)^2 u^2(x_i)}, \tag{A2}$$

where: x is the directly measured parameter.

The air and water densities are assumed to have a standard uncertainty,

$$u(x) = \frac{\Delta_t x^2}{\sqrt{3}}, \tag{A3}$$

where: $\Delta_t x$ is the uncertainty for the tabulated quantities, equal to 10 units of the last decimal place in the tables of physical properties.

The density of Velol-9Q oil was determined by a specialised laboratory and therefore the value declared by the density testing contractor was used as the uncertainty of the oil density.

References

1. Xu, Z.G.; Qu, Z.G.; Zhao, C.Y.; Tao, W.Q. Pool boiling heat transfer on open-celled metallic foam sintered surface under saturation condition. *Int. J. Heat Mass Transf.* **2011**, *54*, 3856–3867. [CrossRef]
2. Kouidri, A.; Madani, B. Thermal and hydrodynamic performance of flow boiling through a heat exchanger filled with various metallic foam samples. *Chem. Eng. Process. Process Intensif.* **2017**, *121*, 162–169. [CrossRef]
3. Hu, H.; Zhu, Y.; Peng, H.; Ding, G.; Sun, S. Effect of tube diameter on pressure drop characteristics of refrigerant–oil mixture flow boiling inside metal-foam filled tubes. *Appl. Therm. Eng.* **2014**, *62*, 433–443. [CrossRef]

4. Abadi, G.B.; Moon, C.; Kim, K.C. Flow boiling visualization and heat transfer in metal-foam-filled mini tubes—Part I: Flow pattern map and experimental data. *Int. J. Heat Mass Transf.* **2016**, *98*, 857–867. [CrossRef]
5. Li, H.-W.; Zhang, C.-Z.; Yang, D.; Sun, B.; Hong, W.-P. Experimental investigation on flow boiling heat transfer characteristics of R141b refrigerant in parallel small channels filled with metal foam. *Int. J. Heat Mass Transf.* **2019**, *133*, 21–35. [CrossRef]
6. Diani, A.; Mancin, S.; Doretti, L.; Rossetto, L. Low-GWP refrigerants flow boiling heat transfer in a 5 PPI copper foam. *Int. J. Multiph. Flow* **2015**, *76*, 111–121. [CrossRef]
7. Zhu, Y.; Hu, H.; Sun, S.; Ding, G. Flow boiling of refrigerant in horizontal metal-foam filled tubes: Part 2—A flow-pattern based prediction method for heat transfer. *Int. J. Heat Mass Transf.* **2015**, *91*, 502–511. [CrossRef]
8. Wang, P.; Liu, D.Y.; Xu, C. Numerical study of heat transfer enhancement in the receiver tube of direct steam generation with parabolic trough by inserting metal foams. *Appl. Energy* **2013**, *102*, 449–460. [CrossRef]
9. Lali, F. A hydrodynamic study of cylindrical metal foam packings: Residence time distribution and two phase pressure drop. *Chem. Eng. Process. Process Intensif.* **2017**, *115*, 1–10. [CrossRef]
10. Jamal-Abad, M.T.; Saedodin, S.; Aminy, M. Experimental investigation on a solar parabolic trough collector for absorber tube filled with porous media. *Renew. Energy* **2017**, *107*, 156–163. [CrossRef]
11. Shi, J.; Zheng, G.; Chen, Z. Experimental investigation on flow condensation in horizontal tubes filled with annular metal foam. *Int. J. Heat Mass Transf.* **2018**, *116*, 920–930. [CrossRef]
12. Azizifar, S.; Ameri, M.; Behroyan, I. Subcooled flow boiling of water in a metal-foam tube: An experimental study. *Int. Commun. Heat Mass Transf.* **2020**, *118*, 104897. [CrossRef]
13. Hu, H.; Zhu, Y.; Ding, G.; Sun, S. Effect of oil on two-phase pressure drop of refrigerant flow boiling inside circular tubes filled with metal foam. *Int. J. Refrig.* **2013**, *36*, 516–526. [CrossRef]
14. Ji, X.; Xu, J. Experimental study on the two-phase pressure drop in copper foams. *Heat Mass Transf.* **2012**, *48*, 153–164. [CrossRef]
15. Zalucky, J.; Wagner, M.; Schubert, M.; Lange, R.; Hampel, U. Hydrodynamics of descending gas-liquid flows in solid foams: Liquid holdup, multiphase pressure drop and radial dispersion. *Chem. Eng. Sci.* **2017**, *168*, 480–494. [CrossRef]
16. Chen, G.; Zhu, X.; Chen, R.; Liao, Q.; Ye, D.; Feng, H.; Liu, J.; Liu, M. Gas–liquid–solid monolithic microreactor with Pd nanocatalyst coated on polydopamine modified nickel foam for nitrobenzene hydrogenation. *Chem. Eng. J.* **2018**, *334*, 1897–1904. [CrossRef]
17. Bao, Z.; Niu, Z.; Jiao, K. Numerical simulation for metal foam two-phase flow field of proton exchange membrane fuel cell. *Int. J. Hydrogen Energy* **2019**, *44*, 6229–6244. [CrossRef]
18. Li, H.-W.; Wei, G.-B.; Wang, Y.-C.; Yang, D.; Sun, B.; Hong, W.-P. Investigation on the phase split characteristics of slug and annular flow in a metal foam-filled T-junction. *Exp. Therm. Fluid Sci.* **2019**, *109*, 109878. [CrossRef]
19. Shadloo, M.S.; Rahmat, A.; Karimipour, A.; Wongwises, S. Estimation of Pressure Drop of Two-Phase Flow in Horizontal Long Pipes Using Artificial Neural Networks. *J. Energy Resour. Technol.* **2020**, *142*, 112110. [CrossRef]
20. Daher, M.A. Development of a Model for Packed foam Fischer-Tropsch Reactors and Optimization through Artificial Neural Networks. Master's Thesis, Politecnico di Milano School of Industrial and Information Engineering, Milan, Italy, 2019.
21. Baiocco, G.; Tagliaferri, V.; Ucciardello, N. Neural Networks Implementation for Analysis and Control of Heat Exchange Process in a Metal Foam Prototypal Device. *Procedia CIRP* **2017**, *62*, 518–522. [CrossRef]
22. Chen, G.; Zhu, X.; Liao, Q.; Chen, R.; Ye, D.; Liu, M.; Wang, K. A novel structured foam microreactor with controllable gas and liquid flow paths: Hydrodynamics and nitrobenzene conversion. *Chem. Eng. Sci.* **2021**, *229*, 116004. [CrossRef]
23. Tourvieille, J.-N.; Philippe, R.; de Bellefon, C. Milli-channel with metal foams under an applied gas–liquid periodic flow: Flow patterns, residence time distribution and pulsing properties. *Chem. Eng. Sci.* **2015**, *126*, 406–426. [CrossRef]
24. Wan, Z.; Sun, Y.; Yang, C.; Kong, X.; Yan, H.; Chen, X.; Huang, T.; Wang, X. Experimental performance investigation on the arrangement of metal foam as flow distributors in proton exchange membrane fuel cell. *Energy Convers. Manag.* **2021**, *231*, 113846. [CrossRef]
25. Gao, W.; Xu, X.; Liang, X. Flow boiling of R134a in an open-cell metal foam mini-channel evaporator. *Int. J. Heat Mass Transf.* **2018**, *126*, 103–115. [CrossRef]
26. Gerbaux, O.; Vercueil, T.; Memponteil, A.; Bador, B. Experimental characterization of single and two-phase flow through nickel foams. *Chem. Eng. Sci.* **2009**, *64*, 4186–4195. [CrossRef]
27. Abadi, G.B.; Moon, C.; Kim, K.C. Flow boiling visualization and heat transfer in metal-foam-filled mini tubes—Part II: Developing predictive methods for heat transfer coefficient and pressure drop. *Int. J. Heat Mass Transf.* **2016**, *98*, 868–878. [CrossRef]
28. Inayat, A.; Schwerdtfeger, J.; Freund, H.; Körner, C.; Singer, R.F.; Schwieger, W. Periodic open-cell foams: Pressure drop measurements and modeling of an ideal tetrakaidecahedra packing. *Chem. Eng. Sci.* **2011**, *66*, 2758–2763. [CrossRef]
29. Weise, S.; Meinicke, S.; Wetzel, T.; Dietrich, B. Modelling the pressure drop of two-phase flow through solid porous media. *Int. J. Multiph. Flow* **2019**, *112*, 13–26. [CrossRef]
30. Akbarnejad, S.; Pour, M.S.; Jonsson, L.T.I.; Jönsson, P.G. Effect of Fluid Bypassing on the Experimentally Obtained Darcy and Non-Darcy Permeability Parameters of Ceramic Foam Filters. *Met. Mater. Trans. B* **2017**, *48*, 197–207. [CrossRef]
31. Kim, D.Y.; Kim, K.C. An experimental study on the thermal and hydraulic characteristics of open-cell nickel and copper foams for compact heat exchangers. *Int. J. Heat Mass Transf.* **2019**, *130*, 162–174. [CrossRef]
32. Lai, Z.; Hu, H.; Ding, G. Influence of pore density on heat transfer and pressure drop characteristics of wet air in hydrophilic metal foams. *Appl. Therm. Eng.* **2019**, *159*, 113897. [CrossRef]

33. Kamath, P.M.; Balaji, C.; Venkateshan, S.P. Experimental investigation of flow assisted mixed convection in high porosity foams in vertical channels. *Int. J. Heat Mass Transf.* **2011**, *54*, 5231–5241. [CrossRef]

34. Dukhan, N.; Suleiman, A.S. Simulation of Entry-Region Flow in Open-Cell Metal Foam and Experimental Validation. *Transp. Porous Media* **2014**, *101*, 229–246. [CrossRef]

35. Dyga, R.; Płaczek, M.; Witczak, S.; Czernek, K. Analysis of Flow Through the Entry Region of a Channel with Metal Foam Packing. In *Practical Aspects of Chemical Engineering. Lecture Notes on Multidisciplinary Industrial Engineering*; Ochowiak, M., Woziwodzki, S., Doligalski, M., Mitkowski, P., Eds.; Springer: Cham, Switzerland, 2018; pp. 101–112.

36. Brol, S.; Czok, R.; Mróz, P. Control of energy conversion and flow in hydraulic-pneumatic system. *Energy* **2020**, *194*, 116849. [CrossRef]

37. Brol, S.; Szegda, A. Magnetism of automotive wheels with pneumatic radial tires. *Measurement* **2018**, *126*, 37–45. [CrossRef]

38. Płaczek, M.; Dyga, R.; Witczak, S. Experimental Investigation of Void Fraction in Horizontal Air-water Flow Through FeCrAlY Foam. *Procedia Eng.* **2012**, *42*, 690–703. [CrossRef]

39. Brol, S.; Dyga, R. Self-affinity approach for the determination of flow regime in pipelines. *Measurement* **2021**, *168*, 108452. [CrossRef]

40. Dyga, R.; Płaczek, M.; Witczak, S. Influence of flow conditions and foam parameters on pressure drop and heat transfer in flow of fluids through channels filled with metal foams. *MATEC Web Conf.* **2018**, *240*, 03005. [CrossRef]

41. Dukhan, N.; Ali, M. Strong wall and transverse size effects on pressure drop of flow through open-cell metal foam. *Int. J. Therm. Sci.* **2012**, *57*, 85–91. [CrossRef]

42. Xu, W.; Zhang, H.; Yang, Z.; Zhang, J. Numerical investigation on the flow characteristics and permeability of three-dimensional reticulated foam materials. *Chem. Eng. J.* **2008**, *140*, 562–569. [CrossRef]

43. Teruel, F.E.; Rizwan-Uddin. Characterization of a porous medium employing numerical tools: Permeability and pressure-drop from Darcy to turbulence. *Int. J. Heat Mass Transf.* **2009**, *52*, 5878–5888. [CrossRef]

44. Troniewski, L.; Dyga, R. Air-water-oil three-phase flow part I. Phenomena of pressure drop depression. *Chem. Process Eng.* **2003**, *24*, 589–599.

45. Dyga, R.; Nowak, M.; Troniewski, L.; Witczak, S. Pressure drop in vertical three-phase flow. *Turbul. Int. J.* **2007**, 123–129.

46. Azzi, W.; Roberts, W.L.; Rabiei, A. A study on pressure drop and heat transfer in open cell metal foams for jet engine applications. *Mater. Des.* **2007**, *28*, 569–574. [CrossRef]

47. Dhiman, S.K.; Verma, V.; Rao, D.P.; Rao, M.S. Process intensification in a trickle-bed reactor: Experimental studies. *AIChE J.* **2005**, *51*, 3186–3192. [CrossRef]

48. Dyga, R.; Płaczek, M. Influence of Hydrodynamic Conditions on the Type and Area of Occurrence of Gas−Liquid Flow Patterns in the Flow Through Open−Cell Foams. *Materials* **2020**, *13*, 3254. [CrossRef]

49. Brol, S.; Mamala, J.J. Application of Spectral and Wavelet Analysis in Power Train System Diagnostic. In Proceedings of the SAE 2010 World Congress, Detroit, MI, USA, 13–15 April 2010.

50. JCGM Evaluation of Measurement Data—Guide to the Expression of Uncertainty in Measurement 2008, 120. Available online: https://isotc.iso.org/livelink/livelink/fetch/2000/2122/4230450/8389141/ISO_IEC_Guide_98%2D3_2008%28E%29_%2D_Uncertainty_of_measurement_%2D%2D_Part_3%2C_Guide_to_the_expression_of_uncertainty_in_measurement_%28GUM%2C1995%29.pdf?nodeid=8389142&vernum=-2 (accessed on 19 April 2021).

51. Jantos, J.; Brol, S.; Mamala, J. Problems in Assessing Road Vehicle Driveability Parameters Determined with the Aid of Accelerometer. In Proceedings of the SAE World Congress & Exhibition, Detroit, MI, USA, 16 April 2007.